ACS APPLIED MATERIALS & INTERFACES

Research Article

www.acsami.org

Development of Cobalt Hydroxide as a Bifunctional Catalyst for Oxygen Electrocatalysis in Alkaline Solution

Yi Zhan,[†] Guojun Du,[‡] Shiliu Yang,[†] Chaohe Xu,[†] Meihua Lu,[†] Zhaolin Liu,[‡] and Jim Yang Lee*,[†]

[†]Department of Chemical and Biomolecular Engineering, National University of Singapore, 10 Kent Ridge Crescent, Singapore 119260, Singapore

[‡]Institute of Materials Research and Engineering, Agency of Science, Technology, and Research (A*STAR), 3 Research Link, Singapore 117602, Singapore

Supporting Information

ABSTRACT: $Co(OH)_2$ in the form of hexagonal nanoplates synthesized by a simple hydrothermal reaction has shown even greater activity than cobalt oxides (CoO and Co_3O_4) in oxygen reduction and oxygen evolution reactions (ORR and OER) under alkaline conditions. The bifunctionality for oxygen electrocatalysis as shown by the OER−ORR potential difference (ΔE) could be reduced to as low as 0.87 V, comparable to the state-of-the-art non-noble bifunctional catalysts, when the $Co(OH)_2$ nanoplates were compounded with nitrogen-doped reduced graphene oxide (N-rGO). The good performance was attributed to the nanosizing of $Co(OH)_2$ and the synergistic interaction between $Co(OH)_2$ and N-rGO. A zinc−air cell assembled with a $Co(OH)_2$−air electrode also showed a performance comparable to that of the state-of-the-art zinc−air cells. The combination of bifunctional activity and operational stability establishes $Co(OH)_2$ as an effective low-cost alternative to the platinum group metal catalysts.

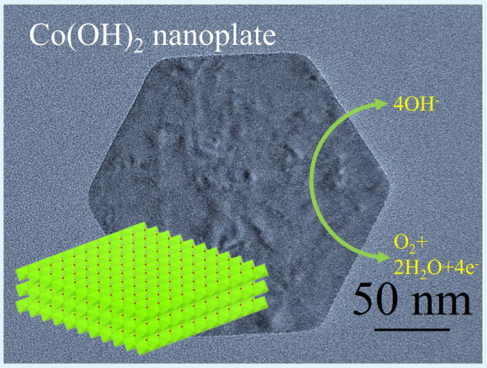

KEYWORDS: *oxygen electrocatalysis, bifunctional catalyst, cobalt hydroxide, zinc−air battery, alkaline solution*

1. INTRODUCTION

The high theoretical energy density of rechargeable metal−air batteries is a draw for the large-scale storage of electrical energy.[1−4] Part of the high energy density is due to oxygen being drawn from the surrounding air and not stored in any form in the battery. The reactions in the air electrode are, however, kinetically challenged,[5] necessitating the use of catalysts to reduce the high overpotentials in these reactions. Because rechargeable metal−air batteries may be regarded as an extension of fuel cells, the platinum group metal (PGM) catalysts, which have a long developmental history and success with fuel cells, were also used as oxygen electrocatalysts in some early rechargeable metal−air systems. The prohibitively high cost of PGMs, however, rules them out as a long-term solution, and the research today is focused on identifying low-cost alternatives to the PGM catalysts.[6,7]

The catalysts for rechargeable metal−air systems are functionally more complex than the catalysts for the fuel cell air electrode. The catalysts have to be active for both the oxygen reduction reaction (ORR) during battery discharge and the oxygen evolution reaction (OER) during battery recharge. Thus, an effective catalyst for the oxygen reactions in rechargeable metal−air batteries is necessarily "bifunctional". A common measure of such bifunctionality is the potential difference (ΔE) between OER and ORR recorded at some current densities of practical significance. Specifically, the ORR potential is often taken at a current density of −3 mA cm^{-2} [about half of the diffusion-limited current density from a standard platinum/carbon (Pt/C) catalyst]. The OER potential, on the other hand, is often taken at a current density of 10 mA cm^{-2}.[6] A small ΔE reflects good catalytic bifunctionality. Bifunctionality in acid and alkaline solutions has been demonstrated by combining several PGMs physically ("cocatalyst system") or chemically ("alloy catalyst system").[8,9] The PGMs, while impractical for actual deployment, are useful, nonetheless, for benchmarking the performance of non-PGM catalysts.

There have been a number of non-PGM catalysts that show stable bifunctionality in oxygen electrocatalysis. The exchange current density is usually higher under alkaline conditions.[7,8,10−12] Many of these catalysts are based on transition-metal oxides.[6,13−16] Among them, $MnCoFeO_4$ supported on nitrogen-doped reduced graphene oxide (N-rGO) has shown the lowest ΔE of 0.93 V, which is only 10 mV higher than that of iridium/carbon (Ir/C), the overall " best" bifunctional catalyst (albeit PGM-based) at a typical total solid loading of 0.1 mg cm^{-2}.[17]

Inspired by recent reports that ORR and OER on metal oxides begin with protonation of the metal oxide surface to form metal hydroxyl species (M−OH),[15,18−20] we envisage the

Received: March 27, 2015
Accepted: May 21, 2015
Published: May 21, 2015

DOI: 10.1021/acsami.5b02670
ACS Appl. Mater. Interfaces 2015, 7, 12930−12936

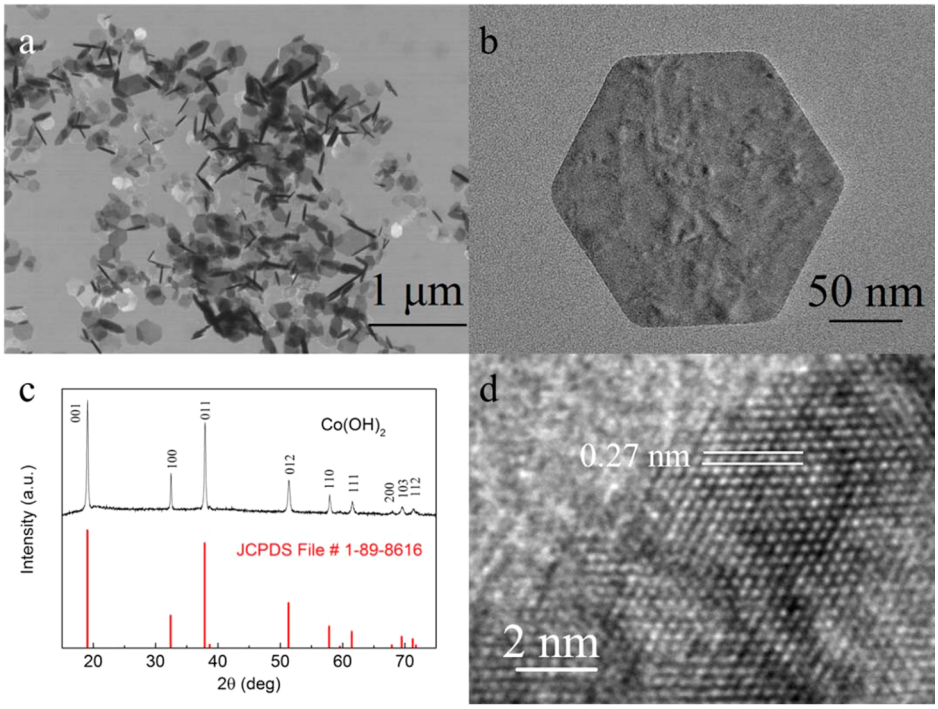

Figure 1. TEM images (a and b), XRD pattern (c), and high-resolution TEM image (d) of the hexagonal $Co(OH)_2$ nanoplates.

possibility of using metal hydroxides directly for bifunctional oxygen electrocatalysis. Because cobalt oxides are the most bifunctional simple oxide catalysts,[14,21−23] cobalt hydroxide would be an interesting candidate to explore. Our literature survey revealed a few studies where $Co(OH)_2$ has been used for ORR, but the performance was generally dismal.[24−27] We noted that the sizes of the hydroxide particles in these studies were rather large (several hundreds of nanometers). There exists the possibility that the application performance may be improved by nanosizing as a result of an increase in the surface area and/or surface reactivity for oxygen electrocatalysis. The hydrothermal synthesis of Liu et al. was able to produce hexagonal $Co(OH)_2$ nanoplates with a lateral side in the tens of nanometers.[28]

This is a report on the development of hexagonal $Co(OH)_2$ nanoplates as a bifunctional oxygen electrocatalyst. The $Co(OH)_2$ nanoplates were found to be more ORR and OER active than CoO and Co_3O_4. ΔE of $Co(OH)_2$ was 0.87 V after compounding with N-rGO. This is comparable to that of the state-of-the-art non-PGM bifunctional catalysts. The value is even lower than those of the previously mentioned $MnCoFeO_4$/N-rGO catalyst and Ir/C.[6,17] Lower cost and a simpler synthesis are the benefits of $Co(OH)_2$ nanoplates over a complex transition-metal oxide such as $MnCoFeO_4$. The good performance of the $Co(OH)_2$ nanoplates was also authenticated in a zinc (Zn)−air battery.

2. EXPERIMENTAL SECTION

2.1. Chemicals. Potassium permanganate ($KMnO_4$, 99%) from Goodrich Chemical Company, cobalt(II) chloride hexahydrate ($CoCl_2{\cdot}6H_2O$, >98.0%), platinum on graphitized carbon (Pt/C, 20 wt %), ruthenium oxide (RuO_2, 99.9%), a hydrogen peroxide solution (H_2O_2, 30%), and triethylamine [$N(CH_2CH_3)_3$, 98%] from Sigma-Aldrich, carbon black (Ketjen black EC 600JD) from Shanghai Tengmin Corp, graphite powder (−200 mesh, 99.9995%) from Alfa-Aesar, and sulfuric acid (H_2SO_4, 98%) and hydrochloric acid (HCl, 37%) from Merck were all used as received. Distilled water was used as the universal solvent.

2.2. Synthesis. Hexagonal $Co(OH)_2$ nanoplates were synthesized by the hydrothermal method of Liu et al.[28] In a typical synthesis, 2 mmol of $CoCl_2{\cdot}6H_2O$ was dissolved in 40 mL of distilled water. A total of 1.0 mL of $N(CH_2CH_3)_3$ was added to the above solution under vigorous stirring. The resultant slurry was transferred to a 50 mL autoclave, sealed, and heated at 180 °C for 20 h in an oven. The autoclave was then left to cool to room temperature naturally. The solid product was recovered, washed with water several times, and freeze-dried. CoO and Co_3O_4 were obtained by calcining the solid product at 400 °C for 2 h in N_2 and in air, respectively.

Nitrogen-doped reduced graphene oxide (N-rGO) was prepared by a previously reported method[17] where graphene oxide from the modified Hummers method was simultaneously reduced and nitrogen-doped by a simple hydrothermal procedure at 150 °C for 3 h. The compounding of N-rGO with $Co(OH)_2$ was based on physical mixing.

2.3. Morphology and Structure of Hydroxides and Oxides. Field-emission transmission electron microscopy (TEM) was performed on a JEOL JEM-2010 transmission electron microscope operating at 200 kV accelerating voltage. X-ray diffraction (XRD) was carried out on a Bruker GADDS XRD powder diffractometer using a Cu Kα source (λ = 1.5418 Å) at 40 kV and 30 mA. N_2 adsorption−desorption isotherms were measured by a Quadrasorb SI surface area and pore size analyzer. Specific surface areas of the samples were calculated by the multipoint Brunauer−Emmett−Teller (BET) method.

2.4. Electrochemical Measurements. A 4.0 mg mL^{-1} catalyst ink was prepared by adding 1.5 mg of catalyst and 3.5 mg of carbon (in the form of carbon black or a mixture of carbon black and N-rGO if stated) to 1.25 mL of a Nafion solution [itself a 1:1:0.08 (v/v) mixture of water, ethanol, and a commercial 5 wt % Nafion solution] followed by 30 min of sonication. A total of 5 μL of the catalyst ink was then drop-cast onto a clean glassy carbon (GC, 5 mm in diameter) electrode to a total solid loading of ∼0.1 mg cm^{-2}. Two PGM electrodes were also prepared to benchmark the catalyst performance: a commercial 20 wt % Pt/C catalyst and a RuO_2 catalyst (a 20 wt % RuO_2−80 wt % carbon black mixture). The total solid loading of PGM electrodes was ∼0.14 mg cm^{-2}. Half-cell electrochemical measurements were performed in a single-compartment glass cell with ∼50 mL

DOI: 10.1021/acsami.5b02670
ACS Appl. Mater. Interfaces 2015, 7, 12930−12936

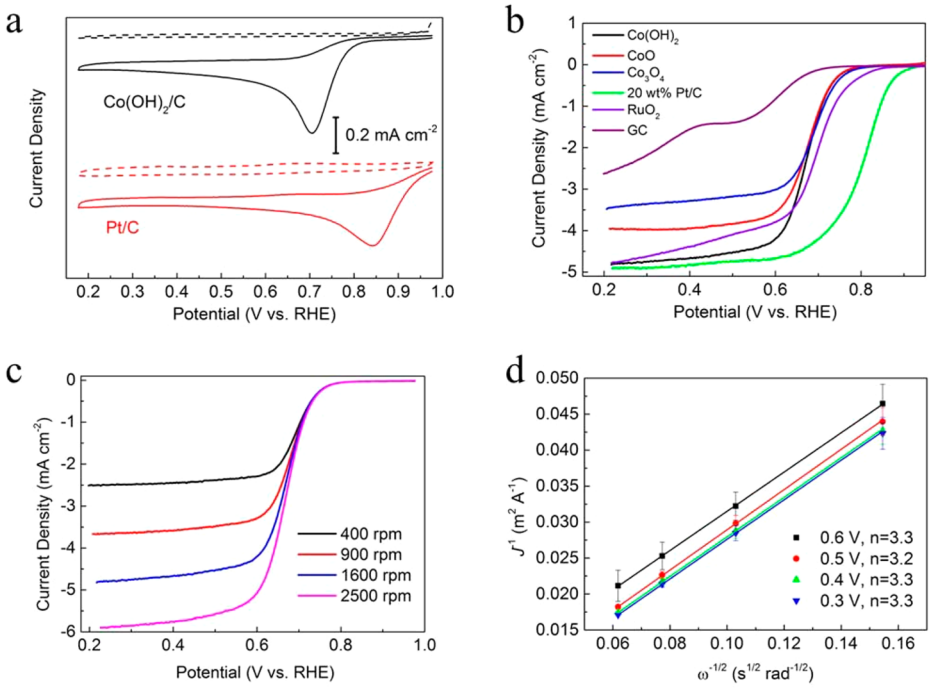

Figure 2. Cyclic voltammograms of $Co(OH)_2$ and Pt/C in N_2-saturated (dashed line) and O_2-saturated (solid line) 0.1 M KOH solutions (a). Polarization curves of ORR on different catalysts at 1600 rpm in an O_2-saturated 0.1 M KOH electrolyte (b). RDE measurements of $Co(OH)_2$ in an O_2-saturated 0.1 M KOH electrolyte at different rotating speeds (c). Corresponding K–L plots (J^{-1} vs $\omega^{-1/2}$, where J is the disk current density and ω is the rotation speed) in the 0.60–0.30 V potential region (d).

of a 0.1 M KOH solution at room temperature. A Ag/AgCl (in 3 M KCl, aq) reference electrode and a platinum foil counter electrode were used together with the GC working electrode to form a standard three-electrode cell. An O_2-saturated environment was maintained during electrochemical measurements by flowing O_2 continuously through the 0.1 M KOH electrolyte. Cyclic voltammetry (CV), linear sweep voltammetry (LSV), and rotating disk electrode (RDE) measurements and chronoamperometry (CA) were performed on an Autolab type III potentiostat/galvanostat. For these measurements, the working electrode was first cycled 10 times to obtain a stable response before data were recorded. The scan rate was 5 mV s^{-1} for CV, LSV, and RDE measurements. All of the potentials in this study were *iR*-corrected and referenced to the reversible hydrogen electrode at pH = 13 [=*E* (V vs Ag/AgCl/3 M KCl) + 0.9783 V]. OER polarization curves were capacitance-corrected before the *iR* correction by taking the average of the anodic and cathodic scans.

Full cell tests were carried out in a custom-made Zn–air cell at room temperature. The air electrode was prepared by drop-casting the catalyst ink into a gas diffusion layer (SGL carbon paper, Germany, 2 cm × 2 cm) to a total solid loading of ~1 mg cm^{-2} (a 30 wt % catalyst–70 wt % carbon mixture). KOH (6 M) was the electrolyte, and the anode was a polished 1-mm-thick Zn plate (Sterling Wire Mesh and Belt Factory). The cells were tested on a Maccor model 4300. The discharge polarization and power density plots were obtained by a galvanodynamic method. Specifically, the cycle stability of the cell was evaluated by charging and discharging at 60 mA for 20 min each per cycle.

3. RESULTS AND DISCUSSION

Hexagonal $Co(OH)_2$ nanoplates were formed under mild hydrothermal synthesis conditions. In the synthesis, $N(CH_2CH_3)_3$ served as both the alkalinity source and complexing agent.[28] TEM imaging showed a large number of uniform hexagonal nanoplates, with a thickness of ~14 nm estimated from the smallest width of the nanorodlike structures when the nanoplates were perpendicular to the view (Figure 1a). An isolated hexagonal nanoplate with a lateral side of ~80 nm is shown in Figure 1b. An aspect ratio of ~5.7 could be calculated from these observations. The XRD pattern of the hexagonal $Co(OH)_2$ nanoplates (Figure 1c) has all of the characteristics of Brucite-like β-$Co(OH)_2$ (JCPDS 1-89-8616). There were no other crystalline phases present, and hence the hydrothermally synthesized product was phase-pure. The 0.27 nm lattice fringes in the TEM image also agree well with diffraction from the $Co(OH)_2$ (100) planes. Heat treatment of the hexagonal $Co(OH)_2$ nanoplates in N_2 and in air transformed them into hexagonal CoO and Co_3O_4 nanoplates with nanosized pores, respectively (Figure S1a,b in the Supporting Information, SI). These pores were likely formed by the removal of –OH groups during pyrolysis.[28] The XRD patterns of the heat-treated $Co(OH)_2$ nanoplates confirm that they were phase-pure CoO (JCPDS 1-70-2855) and Co_3O_4 (JCPDS 42-1467) nanoplates (Figure S1c in the SI). BET measurements showed a notable increase in the specific surface area after heat treatment due to nanopore formation (Figure S2a in the SI).

CV and RDE were first used to determine the pertinent kinetic parameters from ORR and OER on $Co(OH)_2$ nanoplates. Understandably there was no current response from a N_2-saturated 0.1 M KOH solution without oxygen. In an oxygenated 0.1 M KOH solution, on the other hand, the ORR onset and peak potentials on $Co(OH)_2$ were shifted negatively with respect to the reference Sigma Pt/C catalyst (Figure 2a). The lower performance of $Co(OH)_2$ was also apparent in LSV measurements (Figure 2b). As a result, the kinetic mass activity (mass-normalized kinetic current) of $Co(OH)_2$ at 0.9 V was about an order of magnitude lower than that of the Pt/C catalyst (Figure S2b in the SI). By comparison, the ORR activities of CoO and Co_3O_4 are typical of these oxides in the literature[13,14,21,22] and were both lower than that of $Co(OH)_2$, even though there are more Co sites per gram of catalyst in

DOI: 10.1021/acsami.5b02670
ACS Appl. Mater. Interfaces 2015, 7, 12930–12936

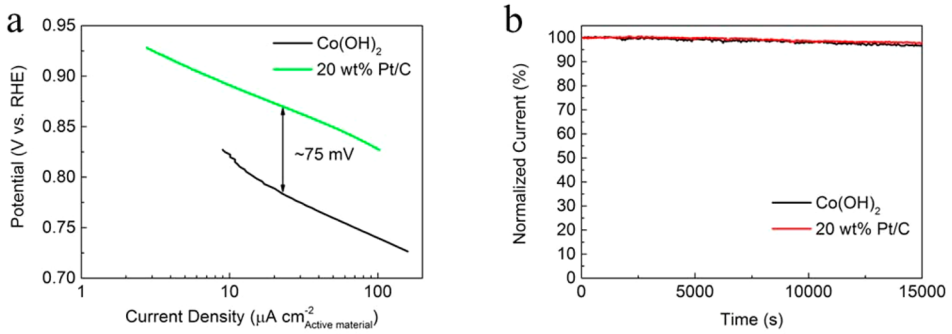

Figure 3. Tafel plots of specific activities of $Co(OH)_2$ and Pt/C for ORR (a). CA of $Co(OH)_2$ and Pt/C dispersed on a carbon paper (0.2 mg cm^{-2}) measured in a O_2-purged 0.1 M KOH solution at 0.70 V and 1600 rpm rotating speed (b).

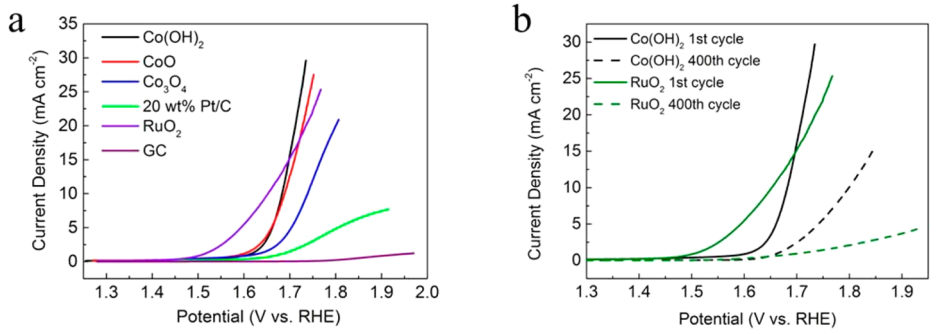

Figure 4. OER polarization curves of different catalysts at 1600 rpm in an O_2-saturated 0.1 M KOH electrolyte (a). Initial OER polarization curves of $Co(OH)_2$ and RuO_2 and OER polarization curves of the same after 400 cycles of CV at 1600 rpm in an O_2-purged 0.1 M KOH solution. The 400 cycles of CV were scanned at 100 mV s^{-1} (b).

CoO and Co_3O_4 and the specific surface areas of CoO and Co_3O_4 are higher than that of $Co(OH)_2$ (Figure S2a in the SI).

The number of electrons in ORR (n) calculated from the Koutecky–Levich (K–L) plot of RDE measurements was ~3.3 for $Co(OH)_2$, indicating the prevalence of a four-electron pathway for ORR on $Co(OH)_2$ between 0.60 and 0.30 V (Figure 2c,d). On the contrary, CoO and Co_3O_4 had lower n values of 2.6–2.7 within the same potential window, verifying that pristine cobalt oxide catalysts are effective mostly for the two-electron pathway of ORR (Figure S3 in the SI).[29,30] $Co(OH)_2$ was therefore the most ORR-active among the three cobalt catalysts in this study. The higher mass activity of $Co(OH)_2$ was mostly due to its higher n value. The higher n value and mass activity of the $Co(OH)_2$ nanoplates than those in earlier studies (Table S1 in the SI) could be attributed to the benefits of nanosizing in providing a larger surface area and a proportional increase in the number of surface defects. The importance of the surface area and surface defects for oxygen electrocatalysis has been established in previous works.[31,32]

The Tafel plots of $Co(OH)_2$ and Pt/C were measured in the 0.73–0.93 V potential region, corresponding to 300–500 mV of overpotential typically found in a Zn–air battery[33] (Figure 3a). Specific activities (kinetic current normalized by the BET area) were used in these plots to filter out the first-order effects of the surface area. The Tafel plots have also been corrected for mass transfer and iR effects to focus on reaction kinetics. The Tafel slope from the linear section of the plot was ~62 mV dec^{-1} for $Co(OH)_2$, close to the ~60 mV dec^{-1} value typically found among Pt/C catalysts.[34,35] This value may be used to infer that ORR on $Co(OH)_2$ in this potential region was rate-limited by the first electron-transfer reaction.[36] Despite the same slope, the Tafel plot of $Co(OH)_2$ was displaced downward by ~75 mV in the voltage direction relative to Pt/C, thereby being about 1 order of magnitude lower in specific activity. Despite the lower ORR activity, $Co(OH)_2$ was as stable as Pt/C in continuous operation for 15000 s (Figure 3b). The reasonably good ORR activity and good stability of $Co(OH)_2$ make this hydroxide a cost- effective alternative to Pt/C for ORR.

$Co(OH)_2$ was also compared with PGM catalysts in OER (Figure 4a). The OER polarization curve was capacitance-corrected by taking the mean of the anodic and cathodic scans and applying iR correction (Figure S4a in the SI). The lowest onset potential for OER in our measurements occurred on RuO_2, followed by $Co(OH)_2$, CoO, and Co_3O_4. RuO_2, however, exhibited a slower incline of the current density with the potential than $Co(OH)_2$, resulting in a higher Tafel slope (Figure S4b in the SI). A high Tafel slope indicates a more sluggish electron transfer during catalysis.[37] It is, however, not uncommon for non-PGM catalysts to have lower Tafel slopes than PGM catalysts in OER.[37,38] Similar to the case of ORR, $Co(OH)_2$ was more OER-active than CoO and Co_3O_4 even though $Co(OH)_2$ had a smaller number of cobalt sites per gram and a smaller surface area. The mass activity of $Co(OH)_2$ nanoplates in the dilute solution of this study was, nonetheless, comparable to previously reported values in more concentrated KOH solutions (Table S2 in the SI). On the other hand, CV measured a higher OER stability for $Co(OH)_2$ relative to that of RuO_2 (Figure 4b).[10] The decrease in the current density after 400 cycles of CV was also lower for $Co(OH)_2$ than RuO_2. The combination of the good activity and good stability of $Co(OH)_2$ suggests that it is a cost-effective alternative to the PGM OER catalysts.

DOI: 10.1021/acsami.5b02670
ACS Appl. Mater. Interfaces 2015, 7, 12930–12936

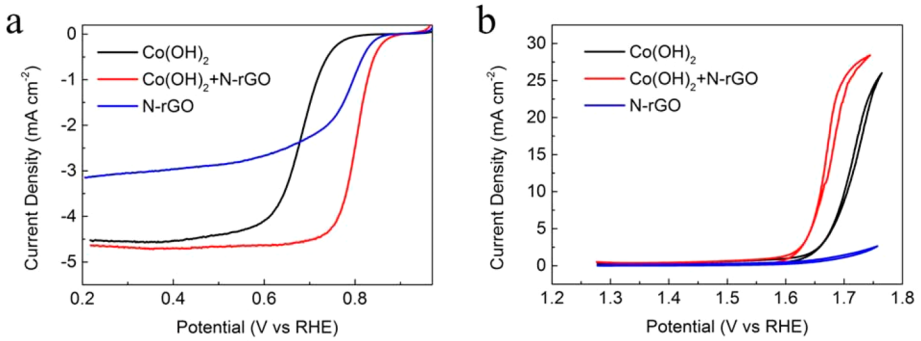

Figure 5. ORR (a) and OER (b) polarization curves of $Co(OH)_2$ + N-rGO (30 wt %−30 wt %) and its constituents at 1600 rpm in an O_2-purged 0.1 M KOH solution.

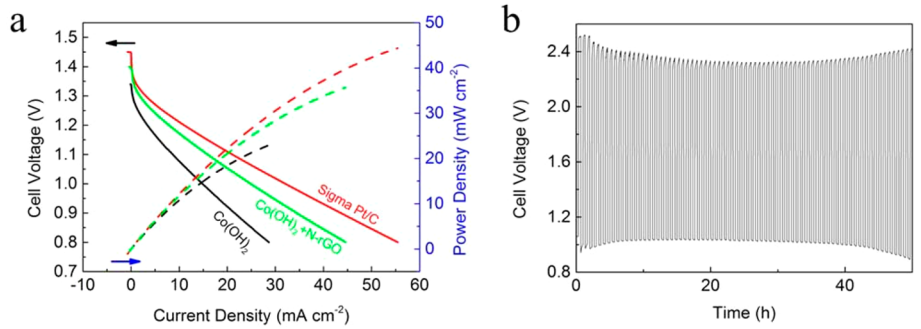

Figure 6. Discharge polarization curves ($V \sim i$) and corresponding power density plots for the Zn−air battery using different air electrodes and a total solid loading of 1 mg cm^{-2} (a). Discharge−charge cycling of the Zn−air battery at 15 mA cm^{-2} with a $Co(OH)_2$ + N-rGO air electrode (b).

The catalyst after the OER stability test was analyzed to understand the cause of performance degradation. XRD measurements indicated the presence of Co_3O_4 instead of $Co(OH)_2$, suggesting that $Co(OH)_2$ was oxidized to Co_3O_4 under prolonged exposure to anodic potentials (Figure S5a in the SI). X-ray photoelectron spectroscopy (XPS) measurements also supported the inference from XRD measurements (Figure S5b in the SI): after the stability test, the binding energies of Co $2p_{1/2}$ and Co $2p_{3/2}$ were negatively shifted from 798.5 and 783.0 eV to 794.8 and 779.8 eV, respectively, and the band separation was also decreased from 15.5 eV for $Co(OH)_2$[39] to 15.0 eV for Co_3O_4,[17] corroborating oxidation of $Co(OH)_2$ to Co_3O_4 as the possible mechanism for degradation of $Co(OH)_2$ under prolonged exposure to the anodic potential region.

The performance of $Co(OH)_2$ nanoplates could be increased further by compounding with N-rGO. N-rGO is a common adjuvant in oxygen electrocatalysts used to improve the performance of the latter through the synergism of intrinsic activity and the reduction of external transport resistance.[17,22] After a series of rudimentary composition adjustments (Figure S6 in the SI), a 30 wt %−30 wt % mixture of $Co(OH)_2$ and N-rGO was found to display the best bifunctional performance. The higher performance of this $Co(OH)_2$−N-rGO composite in ORR and OER than $Co(OH)_2$ or N-rGO alone is confirmation of the synergy (Figure 5). Because both $Co(OH)_2$ and N-rGO are 2D-like materials, their geometrical compatibility ensures a more intimate contact and a greater integration of the two constituents to result in a greater synergy.

When both the ORR and OER performances were taken together, pristine $Co(OH)_2$ showed a ΔE value of 1.02 V, which is smaller (and, hence, more bifunctional) than CoO and Co_3O_4 in this study (Table S3 in the SI). ΔE was reduced further after compounding with N-rGO, where the ΔE value of 0.87 V is comparable to those of the state-of-the-art non-PGM bifunctional catalysts (Table S4 in the SI). There are reports of lower ΔE for the non-PGM catalysts in the literature. However, a high catalyst loading was often used to obtain a high current ensity in these studies. Because the interference from ohmic resistance and mass-transfer limitations is more severe at high catalyst loadings, the results obtained as such are less indicative of the catalyst's intrinsic performance.[40] We have therefore used Ir/C catalysts at a similar low catalyst loading for the ΔE comparison in order to minimize the subjectivity in catalyst performance measurements.

Morphology engineering or cation doping has been the common method used to improve the bifunctional activity of CoO_x. For example, the ordered mesoporous Co_3O_4 of Joo et al. had a ΔE value of 1.03 V at a total solid loading of 0.334 mg cm^{-2}.[14] ΔE was 1.12 V for $MnCoFeO_4$ in our previous study at a total solid loading of 0.1 mg cm^{-2}.[17] What is shown in this study is that good bifunctional activity could be achieved more simply by using hydroxides instead of oxides. Markovic et al. have shown that the OER activity of metal hydr(oxy)oxide is dependent on the bond strength of M−OH, which may explain the good bifunctionality of $Co(OH)_2$ because the Co−OH bond is neither too strong nor too weak.[41] Previous studies have also concluded that oxygen electrocatalysis on metal oxides begins with protonation of the surface metal centers to form M−OH.[15,19,20] The higher performance of $Co(OH)_2$ than both CoO and Co_3O_4 could possibly be due to the removal of a kinetic step in the overall scheme of reactions. This is, however, a hypothesis that requires further examination. $Co(OH)_2$, as an oxide precursor, has naturally a lower cost of production (particularly in comparison with complex oxides such as $MnCoFeO_4$). With good ORR and OER performances and low

DOI: 10.1021/acsami.5b02670
ACS Appl. Mater. Interfaces 2015, 7, 12930−12936

material and production cost, $Co(OH)_2$ is clearly more preferable than oxides as a bifunctional catalyst to compete with PGM-based bifunctional catalysts.

The $Co(OH)_2$ nanoplates were also tested for the air electrode of a custom Zn−air battery. The discharge polarization curve, as measured by the galvanodynamic method, showed significant improvements of the open-circuit voltage, current density, and power density of $Co(OH)_2$ after compounding with N-rGO. The performance of the latter was close to the level of a $MnCoFeO_4$/N-rGO or Pt/C air electrode (Figure 6a). Specifically, the Zn−air battery with a pristine $Co(OH)_2$ air electrode could deliver a current density of ∼29 mA cm^{-2} at 0.8 V, which is comparable to those of the Co_3O_4 and MnO_2 composite electrodes in previous studies. When cycled at a current density of 15 mA cm^{-2} in air (Figure 6b), the Zn−air battery using the $Co(OH)_2$ + N-rGO air electrode could be run for 50 h (75 cycles) continuously with a voltage gap of 1.2−1.3 V and a round trip efficiency of 46%. The longer duration of the operation together with a smaller voltage gap and higher round-trip efficiency is a notable performance upgrade relative to our previous Zn−air cell using the MCF/N-rGO air electrode.[17] This is encouraging because the stability of bifunctional electrodes is often poor and degradation begins within a few cycles of use.[33] It should be mentioned that while the performance of our Zn−air batteries was slightly below binder-free constructions, which have the lowest contact resistance for the air electrode, it is comparable to those of other state-of-the-art Zn−air cells using the drop-cast construction (Table S5 in the SI). On the other hand, the drop-cast electrode construction in this study remains a trusted simpler and cheaper method than binder-free electrode constructions (which may involve hydrothermal processing or electrospinning). Hence, $Co(OH)_2$ nanoplates are capable low-cost non-PGM bifunctional catalysts that can find applications in rechargeable Zn−air batteries.

4. CONCLUSIONS

The hexagonal $Co(OH)_2$ nanoplates synthesized by a simple hydrothermal method demonstrated good activities in OER and ORR, surpassing the performances of CoO and Co_3O_4. The low-cost $Co(OH)_2$ is chemically stable and has a OER−ORR ΔE value as low as 0.87 V after compounding with N-rGO. This is close to those of the state-of-the-art non-PGM bifunctional catalysts. The good bifunctional performance of $Co(OH)_2$ could be attributed to the increased activity of $Co(OH)_2$ due to nanosizing and the integration of $Co(OH)_2$ and N-rGO optimized for the synergy of functions. The results of full cell tests confirmed the viability of using hexagonal $Co(OH)_2$ nanoplates in the air electrode of Zn−air batteries. This study therefore establishes $Co(OH)_2$ as an effective low-cost substitute for PGM catalysts and also as an alternative to improving the activity of cobalt oxide catalysts through the more complex routes of morphology engineering and aliovalent cationic doping.

■ ASSOCIATED CONTENT

Supporting Information

TEM images, XRD patterns, RDE curves, and corresponding K−L plots for CoO and Co_3O_4, BET surface areas for materials, performance comparison with those in the literature for ORR and OER, XPS spectra of $Co(OH)_2$ before and after OER testing, and the effect of the N-rGO content on the catalytic performance. The Supporting Information is available free of charge on the ACS Publications website at DOI: 10.1021/acsami.5b02670.

■ AUTHOR INFORMATION

Corresponding Author

*Tel: 65 65162899. Fax: 65 67791936. E-mail: cheleejy@nus.edu.sg.

Notes

The authors declare no competing financial interest.

■ ACKNOWLEDGMENTS

We thank Thomas Goh and Dr. Xiaoming Ge for their assistance in the Zn−air battery measurements. This work was supported by a grant from the Advanced Energy Storage Program of the Science and Engineering Research Council, Singapore (Grant R-265-000-436-305).

■ REFERENCES

(1) Lee, D. U.; Choi, J. Y.; Feng, K.; Park, H. W.; Chen, Z. W. Advanced Extremely Durable 3d Bifunctional Air Electrodes for Rechargeable Zinc−Air Batteries. *Adv. Energy Mater.* **2014**, *4*, n/a−n/a.

(2) Li, Y.; Gong, M.; Liang, Y.; Feng, J.; Kim, J. E.; Wang, H.; Hong, G.; Zhang, B.; Dai, H. Advanced Zinc−Air Batteries Based on High-Performance Hybrid Electrocatalysts. *Nat. Commun.* **2013**, *4*, 1805−1811.

(3) Lu, J.; Lei, Y.; Lau, K. C.; Luo, X.; Du, P.; Wen, J.; Assary, R. S.; Das, U.; Miller, D. J.; Elam, J. W.; Albishri, H. M.; El-Hady, D. A.; Sun, Y. K.; Curtiss, L. A.; Amine, K. A Nanostructured Cathode Architecture for Low Charge Overpotential in Lithium−Oxygen Batteries. *Nat. Commun.* **2013**, *4*, 2383−2391.

(4) Peng, Z.; Freunberger, S. A.; Chen, Y.; Bruce, P. G. A Reversible and Higher-Rate Li−O_2 Battery. *Science* **2012**, *337*, 563−566.

(5) Lee, J.-S.; Tai Kim, S.; Cao, R.; Choi, N.-S.; Liu, M.; Lee, K. T.; Cho, J. Metal−Air Batteries with High Energy Density: Li−Air Versus Zn−Air. *Adv. Energy Mater.* **2011**, *1*, 34−50.

(6) Gorlin, Y.; Jaramillo, T. F. A Bifunctional Nonprecious Metal Catalyst for Oxygen Reduction and Water Oxidation. *J. Am. Chem. Soc.* **2010**, *132*, 13612−13614.

(7) Liang, Y.; Wang, H.; Zhou, J.; Li, Y.; Wang, J.; Regier, T.; Dai, H. Covalent Hybrid of Spinel Manganese−Cobalt Oxide and Graphene as Advanced Oxygen Reduction Electrocatalysts. *J. Am. Chem. Soc.* **2012**, *134*, 3517−3523.

(8) Jörissen, L. Bifunctional Oxygen/Air Electrodes. *J. Power Sources* **2006**, *155*, 23−32.

(9) Chen, G.; Delafuente, D. A.; Sarangapani, S.; Mallouk, T. E. Combinatorial Discovery of Bifunctional Oxygen Reduction—Water Oxidation Electrocatalysts for Regenerative Fuel Cells. *Catal. Today* **2001**, *67*, 341−355.

(10) Gao, M. R.; Xu, Y. F.; Jiang, J.; Zheng, Y. R.; Yu, S. H. Water Oxidation Electrocatalyzed by an Efficient Mn_3O_4/$CoSe_2$ Nanocomposite. *J. Am. Chem. Soc.* **2012**, *134*, 2930−2933.

(11) Wu, J.; Xue, Y.; Yan, X.; Yan, W. S.; Cheng, Q. M.; Xie, Y. Co_3O_4 Nanocrystals on Single-Walled Carbon Nanotubes as a Highly Efficient Oxygen-Evolving Catalyst. *Nano Res.* **2012**, *5*, 521−530.

(12) Lai, L. F.; Potts, J. R.; Zhan, D.; Wang, L.; Poh, C. K.; Tang, C. H.; Gong, H.; Shen, Z. X.; Jianyi, L. Y.; Ruoff, R. S. Exploration of the Active Center Structure of Nitrogen-Doped Graphene-Based Catalysts for Oxygen Reduction Reaction. *Energy Environ. Sci.* **2012**, *5*, 7936−7942.

(13) Wang, D.; Chen, X.; Evans, D. G.; Yang, W. Well-Dispersed Co_3O_4/Co_2MnO_4 Nanocomposites as a Synergistic Bifunctional Catalyst for Oxygen Reduction and Oxygen Evolution Reactions. *Nanoscale* **2013**, *5*, 5312−5315.

(14) Sa, Y. J.; Kwon, K.; Cheon, J. Y.; Kleitz, F.; Joo, S. H. Ordered Mesoporous Co_3O_4 Spinels as Stable, Bifunctional, Noble Metal-Free Oxygen Electrocatalysts. *J. Mater. Chem. A* **2013**, *1*, 9992−10001.

DOI: 10.1021/acsami.5b02670
ACS Appl. Mater. Interfaces 2015, 7, 12930−12936

(15) Hardin, W. G.; Slanac, D. A.; Wang, X.; Dai, S.; Johnston, K. P.; Stevenson, K. J. Highly Active, Nonprecious Metal Perovskite Electrocatalysts for Bifunctional Metal−Air Battery Electrodes. *J. Phys. Chem. Lett.* **2013**, *4*, 1254−1259.
(16) Du, G.; Liu, X.; Zong, Y.; Hor, T. S.; Yu, A.; Liu, Z. Co_3O_4 Nanoparticle-Modified MnO_2 Nanotube Bifunctional Oxygen Cathode Catalysts for Rechargeable Zinc−Air Batteries. *Nanoscale* **2013**, *5*, 4657−4661.
(17) Zhan, Y.; Xu, C.; Lu, M.; Liu, Z.; Lee, J. Y. Mn and Co Co-substituted Fe_3O_4 Nanoparticles on Nitrogen-Doped Reduced Graphene Oxide for Oxygen Electrocatalysis in Alkaline Solution. *J. Mater. Chem. A* **2014**, *2*, 16217−16223.
(18) Hardin, W. G.; Mefford, J. T.; Slanac, D. A.; Patel, B. B.; Wang, X. Q.; Dai, S.; Zhao, X.; Ruoff, R. S.; Johnston, K. P.; Stevenson, K. J. Tuning the Electrocatalytic Activity of Perovskites through Active Site Variation and Support Interactions. *Chem. Mater.* **2014**, *26*, 3368−3376.
(19) Suntivich, J.; Gasteiger, H. A.; Yabuuchi, N.; Nakanishi, H.; Goodenough, J. B.; Shao-Horn, Y. Design Principles for Oxygen-Reduction Activity on Perovskite Oxide Catalysts for Fuel Cells and Metal−Air Batteries. *Nat. Chem.* **2011**, *3*, 546−550.
(20) Suntivich, J.; May, K. J.; Gasteiger, H. A.; Goodenough, J. B.; Shao-Horn, Y. A Perovskite Oxide Optimized for Oxygen Evolution Catalysis from Molecular Orbital Principles. *Science* **2011**, *334*, 1383−1385.
(21) Liang, Y.; Wang, H.; Diao, P.; Chang, W.; Hong, G.; Li, Y.; Gong, M.; Xie, L.; Zhou, J.; Wang, J.; Regier, T. Z.; Wei, F.; Dai, H. Oxygen Reduction Electrocatalyst Based on Strongly Coupled Cobalt Oxide Nanocrystals and Carbon Nanotubes. *J. Am. Chem. Soc.* **2012**, *134*, 15849−15857.
(22) Liang, Y.; Li, Y.; Wang, H.; Zhou, J.; Wang, J.; Regier, T.; Dai, H. Co_3O_4 Nanocrystals on Graphene as a Synergistic Catalyst for Oxygen Reduction Reaction. *Nat. Mater.* **2011**, *10*, 780−786.
(23) Masa, J.; Xia, W.; Sinev, I.; Zhao, A.; Sun, Z.; Grutzke, S.; Weide, P.; Muhler, M.; Schuhmann, W. Mn_xO_y/Nc and Co_xO_y/Nc Nanoparticles Embedded in a Nitrogen-Doped Carbon Matrix for High-Performance Bifunctional Oxygen Electrodes. *Angew. Chem., Int. Ed.* **2014**, *53*, 8508−8512.
(24) Liu, Z. X.; Li, Z. P.; Qin, H. Y.; Liu, B. H. Oxygen Reduction Reaction Via the 4-Electron Transfer Pathway on Transition Metal Hydroxides. *J. Power Sources* **2011**, *196*, 4972−4979.
(25) Wu, J.; Zhang, D.; Wang, Y.; Wan, Y.; Hou, B. Catalytic Activity of Graphene−Cobalt Hydroxide Composite for Oxygen Reduction Reaction in Alkaline Media. *J. Power Sources* **2012**, *198*, 122−126.
(26) Dinamani, M.; Kamath, P. V. Electrocatalysis of Oxygen Evolution at Stainless Steel Anodes by Electrosynthesized Cobalt Hydroxide Coatings. *J. Appl. Electrochem.* **2000**, *30*, 1157−1161.
(27) Elumalai, P.; Vasan, H.; Munichandraiah, N. Electrochemical Studies of Cobalt Hydroxide—an Additive for Nickel Electrodes. *J. Power Sources* **2001**, *93*, 201−208.
(28) Liu, X.; Yi, R.; Zhang, N.; Shi, R.; Li, X.; Qiu, G. Cobalt Hydroxide Nanosheets and Their Thermal Decomposition to Cobalt Oxide Nanorings. *Chem.—Asian J.* **2008**, *3*, 732−738.
(29) Wang, Y.; Lu, X.; Liu, Y.; Deng, Y. Silver Supported on Co_3O_4 Modified Carbon as Electrocatalyst for Oxygen Reduction Reaction in Alkaline Media. *Electrochem. Commun.* **2013**, *31*, 108−111.
(30) He, Q. G.; Li, Q.; Khene, S.; Ren, X. M.; Lopez-Suarez, F. E.; Lozano-Castello, D.; Bueno-Lopez, A.; Wu, G. High-Loading Cobalt Oxide Coupled with Nitrogen-Doped Graphene for Oxygen Reduction in Anion-Exchange-Membrane Alkaline Fuel Cells. *J. Phys. Chem. C* **2013**, *117*, 8697−8707.
(31) Cheng, F.; Shen, J.; Peng, B.; Pan, Y.; Tao, Z.; Chen, J. Rapid Room-Temperature Synthesis of Nanocrystalline Spinels as Oxygen Reduction and Evolution Electrocatalysts. *Nat. Chem.* **2011**, *3*, 79−84.
(32) Oh, S. H.; Black, R.; Pomerantseva, E.; Lee, J.-H.; Nazar, L. F. Synthesis of a Metallic Mesoporous Pyrochlore as a Catalyst for Lithium−O_2 Batteries. *Nat. Chem.* **2012**, *4*, 1004−1010.
(33) Li, Y.; Dai, H. Recent Advances in Zinc−Air Batteries. *Chem. Soc. Rev.* **2014**, *43*, 5257−5275.
(34) Suntivich, J.; Gasteiger, H. A.; Yabuuchi, N.; Shao-Horn, Y. Electrocatalytic Measurement Methodology of Oxide Catalysts Using a Thin-Film Rotating Disk Electrode. *J. Electrochem. Soc.* **2010**, *157*, B1263−B1268.
(35) Xu, C.; Zhang, Y.; Wang, L.; Xu, L.; Bian, X.; Ma, H.; Ding, Y. Nanotubular Mesoporous Pdcu Bimetallic Electrocatalysts toward Oxygen Reduction Reaction. *Chem. Mater.* **2009**, *21*, 3110−3116.
(36) Jiang, L.; Hsu, A.; Chu, D.; Chen, R. A Highly Active Pd Coated Ag Electrocatalyst for Oxygen Reduction Reactions in Alkaline Media. *Electrochim. Acta* **2010**, *55*, 4506−4511.
(37) Song, F.; Hu, X. Exfoliation of Layered Double Hydroxides for Enhanced Oxygen Evolution Catalysis. *Nat. Commun.* **2014**, *5*, 4477−4485.
(38) Gong, M.; Li, Y.; Wang, H.; Liang, Y.; Wu, J. Z.; Zhou, J.; Wang, J.; Regier, T.; Wei, F.; Dai, H. An Advanced Ni−Fe Layered Double Hydroxide Electrocatalyst for Water Oxidation. *J. Am. Chem. Soc.* **2013**, *135*, 8452−8455.
(39) Li, Z. P.; Wang, J. Q.; Niu, L. Y.; Sun, J. F.; Gong, P. W.; Hong, W.; Ma, L. M.; Yang, S. R. Rapid Synthesis of Graphene/Cobalt Hydroxide Composite with Enhanced Electrochemical Performance for Supercapacitors. *J. Power Sources* **2014**, *245*, 224−231.
(40) Shin, D.; Jeong, B.; Choun, M.; Ocon, J. D.; Lee, J. Diagnosis of the Measurement Inconsistencies of Carbon-Based Electrocatalysts for the Oxygen Reduction Reaction in Alkaline Media. *RSC Adv.* **2015**, *5*, 1571−1580.
(41) Subbaraman, R.; Tripkovic, D.; Chang, K.-C.; Strmcnik, D.; Paulikas, A. P.; Hirunsit, P.; Chan, M.; Greeley, J.; Stamenkovic, V.; Markovic, N. M. Trends in Activity for the Water Electrolyser Reactions on 3d M(Ni,Co,Fe,Mn) Hydr(Oxy)Oxide Catalysts. *Nat. Mater.* **2012**, *11*, 550−557.

DOI: 10.1021/acsami.5b02670
ACS Appl. Mater. Interfaces 2015, 7, 12930−12936